^{110,116}Cd(α,α)^{110,116}Cd elastic scattering and systematic investigation of elastic α scattering cross sections along the $Z = 48$ isotopic and $N = 62$ isotonic chains

G. G. Kiss,[1,*] P. Mohr,[1,2] Zs. Fülöp,[1] Gy. Gyürky,[1] Z. Elekes,[1] J. Farkas,[1] E. Somorjai,[1] C. Yalcin,[1,3] D. Galaviz,[4,†] R. T. Güray,[3] N. Özkan,[3] and J. Görres[5]

[1]*Institute of Nuclear Research, Hungarian Academy of Sciences, H-4001 Debrecen, P.O. Box 51, Hungary*

[2]*Diakonie-Klinikum, D-74523 Schwäbisch Hall, Germany*

[3]*Department of Physics, Kocaeli University, TR-41380 Umuttepe, Kocaeli, Turkey*

[4]*Instituto de Estructura de la Materia, Consejo Superior de Investigaciones Cientificas, E-28006 Madrid, Spain*

[5]*University of Notre Dame, South Bend, Indiana 46556, USA*

(Received 14 February 2011; published 23 June 2011)

The elastic scattering cross sections for the reactions ^{110,116}Cd(α,α)^{110,116}Cd at energies above and below the Coulomb barrier are presented to provide a sensitive test for the α-nucleus optical potential parameter sets. Additional constraints for the optical potential are taken from the analysis of elastic scattering excitation functions at backward angles which are available in literature. Moreover, the variation of the elastic α scattering cross sections along the $Z = 48$ isotopic and $N = 62$ isotonic chain is investigated by the study of the ratios of the ^{106,110,116}Cd(α,α)^{106,110,116}Cd scattering cross sections at $E_{\rm cm} \approx 15.6$ and 18.8 MeV and the ratio of the ^{110}Cd(α,α)^{110}Cd and ^{112}Sn(α,α)^{112}Sn reaction cross sections at $E_{\rm cm} \approx 18.8$ MeV, respectively. These ratios are sensitive probes for the α-nucleus optical potential parametrizations. The potentials under study are a basic prerequisite for the prediction of α-induced reaction cross sections (e.g., for the calculation of stellar reaction rates in the astrophysical p or γ process).

DOI: 10.1103/PhysRevC.83.065807 PACS number(s): 24.10.Ht, 25.55.Ci, 26.30.−k

I. INTRODUCTION

Most of the nuclei heavier than iron are built up via neutron capture reactions in the so-called s and r processes. However, on the proton-rich side of the valley of stability there are 35 proton-rich nuclei not created by neutron capture processes. These mostly even-even proton-rich, stable isotopes between ^{74}Se and ^{196}Hg are the so-called p nuclei [1]. Their natural isotopic abundance is 10 to 100 times less than that of the more abundant neutron-rich isotopes that were synthesized in the s or r processes.

In the production of the p nuclei, photon-induced reactions at temperatures around a few gigakelvin are playing a crucial role. It is generally accepted that the main stellar mechanism synthesizing these nuclei—the so-called γ process—is initiated by (γ,n) photodisintegration reactions on preexisting neutron-rich s and r seed nuclei. Photons with high energy and high flux, necessary for the γ-induced reactions, are available in explosive nucleosynthesis scenarios, as in the Ne/O burning layer in type II supernovae [1,2]. As the neutron separation energy increases along the (γ,n) path toward more neutron deficient isotopes, (γ,p) and (γ,α) reactions become more important and process the material toward lower atomic numbers [2–5]. Recently, consistent studies of p nucleosynthesis have become available, employing theoretical reaction rates in large reaction networks [3,4]. These studies confirmed that, in the case of the heavy p nuclei ($140 \leqslant A \leqslant 200$), ($\gamma$,$n$) and ($\gamma$,$\alpha$) reactions play the dominant role.

Modeling the synthesis of the p nuclei and calculating their abundances requires an extended reaction network involving more than 10^4 reactions on 2000 mostly unstable nuclei. The reaction rates are usually based on the Hauser-Feshbach statistical model. Because of the experimental challenges very few (γ,α) studies have been performed until now: in a recent experiment the cross section of the ^{144}Sm(γ,α)^{140}Nd has been measured [6]. However, in such an experiment the target nucleus is always in its ground state, whereas in stellar environments thermally populated excited states also contribute to the reaction rate. Thus theoretical considerations cannot be avoided [7]. Alternatively, the (γ,α) rates can be determined experimentally by measuring the inverse (α,γ) reaction cross section and converting the results by using the detailed balance theorem. In this direction the influence of thermally excited states remains relatively small [7,8]. In recent years a range of (α,γ) reaction cross sections on ^{70}Ge, ^{96}Ru, ^{106}Cd, ^{112,117}Sn, ^{113}In, ^{144}Sm, ^{151}Eu, and ^{169}Tm has been measured using the activation method, and the results have been compared with model predictions [9–17].

It was generally found that the (γ,α) and (α,γ) reaction cross section calculations are very sensitive to the choice of the α-nucleus potential, which is a sum of a Coulomb and a nuclear part (the latter one consists of a real and an imaginary part). The cross section predictions using different global α-nucleus optical potential parametrizations can differ within an order of magnitude [12]. Since the parameters of the global α-nucleus optical potentials are usually determined from the analysis of the angular distributions of elastically scattered α particles (and are adjusted to α-induced cross sections if experimental

*ggkiss@atomki.hu; Present address: Laboratori Nazionali del Sud, INFN, Catania, Italia.

†Present address: Centro de Física Nuclear da Universidade de Lisboa, 1649-003, Lisbon, Portugal.

data exist), the elastic α scattering cross sections on several p nuclei has been measured in recent years at the Institute of Nuclear Research of the Hungarian Academy of Sciences (ATOMKI) [18–22] and similar experiments are ongoing at Notre Dame University [23].

In order to increase our knowledge of the α-nucleus optical potential parametrizations, the energy and the mass dependence of the potential parameters has to be understood. Although it would be helpful to perform systematic investigations on the α-nucleus optical potential parametrizations in the whole mass range of the p nuclei (i.e., from about $A \approx 70$ up to almost $A \approx 200$), the fact that most of these nuclei have low-lying first excited states makes a study of elastic scattering experimentally very difficult. Experimental studies are well accessible in the region of the lower mass p nuclei in the $A \approx 100$ mass range and around $A \approx 140$–150 where relatively high-lying first excited states are found. Here the features of the optical potential parameterizations should be as well understood as possible. However, as a word of caution, one should to keep in mind that high-lying first excited states are related to shell closures (e.g., $Z = 50$ and $N = 82$ in these mass regions) and the imaginary part of the optical potential is typically smaller for closed-shell nuclei than for nuclei off closed shell. It is one motivation of the present investigation to study the optical potential for nuclei without closed shells.

From the astrophysical point of view, the potential parameters should be derived in the relevant energy region, in the so-called Gamow window. However, at those sub-Coulomb energies the elastic scattering cross sections are practically not deviating from the Rutherford cross section and for this reason it is not possible to derive reliable optical potential parameters for these energies. Consequently, the experiments have to be performed at slightly higher energies just below and above the Coulomb barrier and then the resulting optical potential parameters have to be extrapolated down to the relevant energy region. Contrary to the real part of the nuclear potential which has a smooth energy dependence, the imaginary part changes drastically around the Coulomb barrier.

A global α-nucleus optical potential must be able not only to provide a correct prediction for the α elastic scattering angular distributions but also to describe the variation of the angular distributions along isotopic and isotonic chains. This is especially important for the extrapolation to unstable nuclei where no measured α-induced reaction data are available and the potential cannot be derived from experimental scattering data. Recently, the variation of the scattering cross sections along the $Z = 50$ isotopic and $N = 50$ isotonic chain has been investigated. The ratio of the measured cross sections of the ^{112}Sn$(\alpha,\alpha)^{112}$Sn/^{124}Sn$(\alpha,\alpha)^{124}$Sn ($Z = 50$) and ^{89}Y$(\alpha,\alpha)^{89}$Y/^{92}Mo$(\alpha,\alpha)^{92}$Mo ($N = 50$) reactions showed an oscillation pattern at backward angles. It was found that both regional and global α-nucleus optical potential parametrizations failed to reproduce these oscillation patterns [22,24].

In order to further investigate the variation of the elastic α scattering cross sections along isotopic and isotonic chains, in the present work the ^{110,116}Cd$(\alpha,\alpha)^{110,116}$Cd reactions are studied at energies above and below the Coulomb barrier.

This paper is organized as follows. In Sec. II we describe our experimental procedure. The measured angular distributions are compared to predictions using local (Sec. III), regional, and global optical potential parametrizations in Sec. IV. Excitation functions taken from literature [25–27] provide further information on the potentials; the experimental excitation functions are compared to the results from the local, regional, and global potentials in Sec. V. Additionally, all calculations are used to predict the ratio of angular distributions along the cadmium ($Z = 48$) isotopic and $N = 62$ isotonic chains (Sec. VI). The elastic α scattering cross sections of the ^{106}Cd$(\alpha,\alpha)^{106}$Cd and the ^{112}Sn$(\alpha,\alpha)^{112}$Sn are taken from [20–22]. A further detailed study on ^{106}Cd$(\alpha,\alpha)^{106}$Cd elastic scattering and the influence of the chosen potential on α-induced cross sections of ^{106}Cd will be presented in a separate paper [28].

II. EXPERIMENTAL PROCEDURE

The experiment was carried out at the cyclotron laboratory of ATOMKI, Debrecen. A similar experimental setup was used also in the previous experiments [18,19,21,22,24] and is described in more detail in [29,30]. The proton and neutron number, the energy of the first excited states of the target nuclei, and the energies of the measured angular distributions are summarized in Table I. The following paragraphs provide a short description of the experimental setup.

The targets were produced by evaporating highly enriched ($\geqslant 95\%$) ^{110,116}Cd onto thin carbon foils ($\approx 20\ \mu$g/cm^2). The target thickness was approximately 200 μg/cm^2, determined via α particle energy loss measurement using radioactive sources. The targets were mounted on a remotely controlled target ladder in the center of the scattering chamber. Figure 1 illustrates the scattering chamber.

The energies of the α beam were 16.14 and 19.46 MeV with typical beam currents of 150–200 pnA. An aperture of 2×6 mm was mounted on the target ladder to check the beam position and size of the beamspot before and after every change

TABLE I. Charge and neutron number, energy of the first excited state of the target nuclei, enrichment, and $E_{\rm lab}$ and $E_{\rm cm}$ energies for each of the angular distributions studied in the present work, the ^{106}Cd and ^{112}Sn data are taken from [20–22]. The nuclear data are from [31–34].

target nuclei	proton number	neutron number	first excited state (keV)	enrichment (%)	$E_{\rm lab}$ (MeV)	$E_{\rm cm}$ (MeV)	Ref.
^{110}Cd	48	62	657.76	95.7	16.14, 19.46	15.6, 18.8	this paper
^{116}Cd	48	68	513.49	98.3	16.14, 19.46	15.6, 18.8	this paper
^{106}Cd	48	58	632.64	96.5	16.13, 19.61	15.6, 18.9	[20,21]
^{112}Sn	50	62	1256.85	99.8	19.51	18.8	[22]

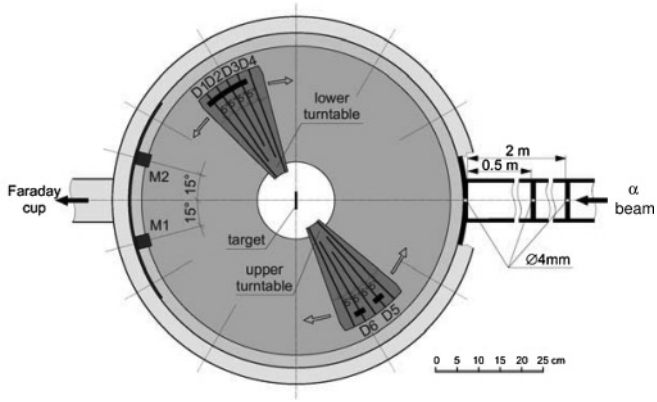

FIG. 1. Schematic view of the scattering chamber with monitor detectors (M1 and M2, mounted in the wall of the chamber at fixed $\pm$ 15° angles) and detectors (D1–D6 on the two turntables) used to measure the yield of the elastically scattered α particles. For details, see text.

of the beam energy or current. We optimized the beam until not more than 1% of the total beam current could be measured on this aperture. As a result of the procedure, the horizontal size of the beamspot was below 2 mm during the whole experiment, which is crucial for the precise determination of the scattering angle. Since the imaginary part of the optical potential depends sensitively on the energy, it is important to have a well-defined beam energy. Therefore the beam was collimated by tight slits (1 mm wide) after the analyzing magnet; this corresponds to an overall energy spread of around 100 keV which is the dominating contribution of the energy resolution of the spectra (see Fig. 2). Six ion-implanted silicon detectors with active areas of 50 mm^2 were used to measure the angular distributions. Their solid angles varied between 1.45×10^{-4} and 1.87×10^{-4}. The detectors were mounted on two turntables. Two detectors with angular distance of 10° were mounted onto the upper turntable and were used to measure the scattering cross sections at forward angles. To measure the cross sections at backward angles four detectors with angular distance of 5° were used. The ratio of their solid angles was determined by measurements at overlapping angles with good statistics ($\leqslant$1% uncertainty). Typical spectra are shown in Fig. 2. As can be seen, the relevant peaks from elastic ^{110,116}Cd α scattering are well separated at all angles from elastic and inelastic peaks of target contaminations as well as from the inelastic α scattering on Cd isotopes. In addition, two detectors were mounted at a larger distance on the wall of the scattering chamber at fixed angles $\vartheta = \pm 15°$ left and right to the beam axis. These detectors were used as monitor detectors (their solid angles were 1.1×10^{-6}) during the whole experiment to normalize the measured angular distribution and to determine the precise position of the beam on the target.

Knowledge of the exact angular position of the detectors is of crucial importance for the precision of a scattering experiment since the Rutherford cross section depends sensitively on the angle specially at forward directions. The uncertainty in the angular distribution is dominated by the error of the scattering angles in the forward region. To determine the scattering angle precisely, we measured kinematic coincidences between

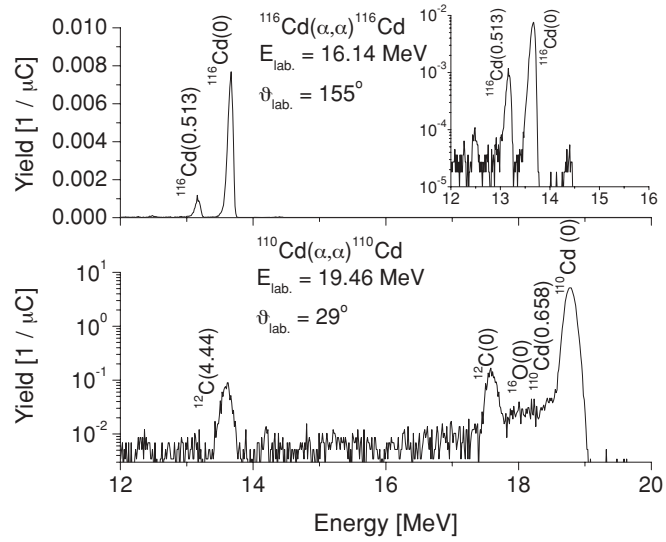

FIG. 2. Typical spectra of the ^{116}Cd(α,α)^{116}Cd and ^{110}Cd(α,α)^{110}Cd reactions at $E_{\rm lab} = 16.14$ MeV (upper part) and $E_{\rm lab} = 19.46$ MeV (lower part), respectively. The upper spectrum was taken at $\vartheta_{\rm lab} = 155°$ (the inset shows the spectrum on logarithmic scale), the lower one at $\vartheta_{\rm lab} = 29°$. It can be seen that there are more than two orders of magnitude difference in the elastic scattering cross sections. The peak from elastic ^{116}Cd α and ^{110}Cd α scattering is well resolved from the inelastic events and from both the ^{12}C α and ^{16}O α elastic scattering.

elastically scattered α particles and the corresponding ^{12}C recoil nuclei using a pure carbon backing as target. One detector was placed at $\vartheta = 70°$, and the signals from the elastically scattered α particles on ^{12}C were selected as gates for the other detector which moved around the expected ^{12}C recoil angle $\vartheta = 45.83°$. We repeated this process for all detector pairs. Figure 3 shows the relative yield of the ^{12}C recoil nuclei in coincidence with elastically scattered α particles as a

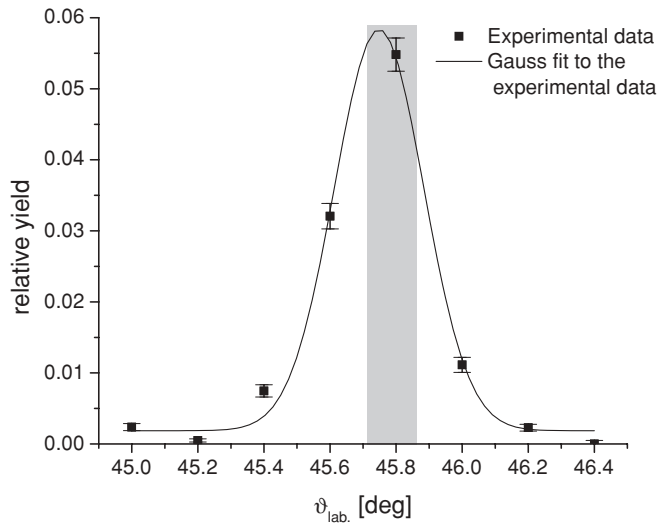

FIG. 3. Relative yield of ^{12}C recoil nuclei in coincidence with elastically scattered α particles. A Gaussian fit fitted to the experimental data is shown to guide the eye. The shaded area represents the angular uncertainty.

function of the ^{12}C recoil angle. The final angular uncertainty was found to be $\Delta\vartheta \leqslant 0.12^\circ$.

Complete angular distributions between 20° and 175° were measured at energies of $E_{lab} = 16.14$ and 19.46 MeV in 1° ($20^\circ \leqslant \vartheta \leqslant 100^\circ$) and 2.5° ($100^\circ \leqslant \vartheta \leqslant 175^\circ$) steps. The statistical uncertainties varied between 0.1% (forward angles) and 4% (backward angles). The count rates $N(\vartheta)$ have been normalized to the yield of the monitor detectors $N_{Mon}(\vartheta = 15^\circ)$:

$$\left(\frac{d\sigma}{d\Omega}\right)(\vartheta) = \left(\frac{d\sigma}{d\Omega}\right)_{Mon} \frac{N(\vartheta)}{N_{Mon}} \frac{\Delta\Omega_{Mon}}{\Delta\Omega}, \quad (1)$$

with $\Delta\Omega$ being the solid angles of the detectors. Whereas the Rutherford-normalized cross sections cover only about two orders of magnitude between the highest (forward angles at $E_{lab} = 16.14$ MeV) and the lowest cross sections (backward angles at $E_{lab} = 19.46$ MeV), the underlying cross sections cover more than four orders of magnitude. Over this huge range of cross sections almost the same accuracy of about 4–5 % total uncertainty could be achieved. This error is mainly caused by the uncertainty of the determination of the scattering angle in the forward region and from the statistical uncertainty in the backward region.

The origin of the above uncertainties has to be studied in further detail. The uncertainty of the scattering angle is composed of two fractions. First, a systematic uncertainty comes from the alignment of the angular scale and the beam direction; it affects all data points in the same direction. This uncertainty is partly compensated by the absolute normalization of the data (see below) where the data are adjusted to Rutherford scattering at forward angles. Second, the accuracy of the setting or reading of the angle leads to a statistical uncertainty, obviously different for each data point. The combination of both remains below 4–5 %. From the small scatter of the data points (see Fig. 4) it may be estimated that the systematic contribution dominates the real uncertainties. Because the statistical uncertainties are smaller than the shown error bars, it must be expected that the resulting χ^2/F may be even below 1.0 for the locally adjusted potentials (see Sec. III).

The absolute normalization is done in two steps. In the first step the absolute normalization is taken from experiment (i.e., from the integrated beam current, the solid angle of the detectors, and the thickness of the target). This procedure has a relatively large uncertainty of the order of 10% which is mainly based on the uncertainties of the target thickness. In a second step a fine tuning of the absolute normalization is obtained by comparison to theoretical calculations at very forward angles. It is obvious that calculated cross sections from any reasonable potential do not deviate practically from the Rutherford cross section at the most forward angles of this experiment; typical deviations are below 0.5% for all potentials listed in Secs. III and IV (including those potentials that do not describe details of the angular distributions at backward angles). This fine tuning changed the first experimental normalization by only 2.5% and thus confirmed the first normalization within the given errors.

The measured angular distributions are shown in Fig. 4. The ^{106}Cd(α,α)^{106}Cd data, are taken from [20,21]. The lines are the results of optical model predictions using local, regional and global α-nucleus potentials (see discussion in the following Secs. III and IV).

III. LOCAL α-NUCLEUS OPTICAL POTENTIAL

The complex optical model potential (OMP) $U(r)$ is given by

$$U(r) = V_C(r) + V(r) + iW(r), \quad (2)$$

where $V_C(r)$ is the Coulomb potential, and $V(r)$ and $W(r)$ are the real and the imaginary parts of the nuclear potential, respectively. The volume integrals per interacting nucleon pair J_R and J_I are defined as usual. Although J_R and J_I are negative (attractive real potential and absorption by the imaginary potential), in the discussion the negative signs are omitted (as usual).

The $V(r)$ real part of the local optical potential is derived from the double-folding model. For calculating the $V_F(r)$ folding potential the density-dependent $M3Y$ interaction [35–37] was used,

$$V(r) = \lambda\, V_F(r/w), \quad (3)$$

where $\lambda \approx 1.1$–1.4 is the potential strength parameter [38] and $w = 1.0 \pm 0.05$ is the width parameter that slightly modifies the potential width. (Larger deviations of the width parameter w from unity would indicate a failure of the folding potential.) The nuclear densities are derived from the compilation of charge densities measured by electron scattering [39]. Thus, we have only two adjustable parameters (λ and w) in the real part of the potential (e.g., compared to three parameters for Woods-Saxon potentials) and, in addition, the range of these parameters is very restricted from the systematics of volume integrals J_R [38] and the above requirement $w \approx 1$.

The Coulomb potential is taken in the usual approximation of a homogeneously charged sphere. The Coulomb radius R_C is equal to the root-mean-square (rms) radius of the folding potential with $w = 1$.

The imaginary part $W(r)$ of the potential is taken in the usual Woods-Saxon parametrization. For the fits to the experimental data we use volume and surface potentials

$$W(r) = W_V \times f(x_V) + 4\, W_S \times \frac{df(x_S)}{dx_S} \quad (4)$$

with the potential depths W_V and W_S of the volume and surface parts and

$$f(x_i) = \frac{1}{1 + \exp(x_i)} \quad (5)$$

and $x_i = [r - R_i\,(A_T^{1/3})]/a_i$ with the radius parameters R_i in the light-ion convention, the diffuseness parameters a_i, and $i = S, V$. It is well established that at very low energies the surface contribution of the imaginary part is dominating; e.g., in [22] it is suggested that the surface contribution is about 80% for α scattering of the neighboring nuclei ^{112}Sn and ^{124}Sn at energies below 20 MeV. At higher energies (i.e., significantly above the Coulomb barrier) the volume contribution is dominating. Whereas for ^{106}Cd a small imaginary volume contribution was found [20], the angular distributions for ^{110}Cd

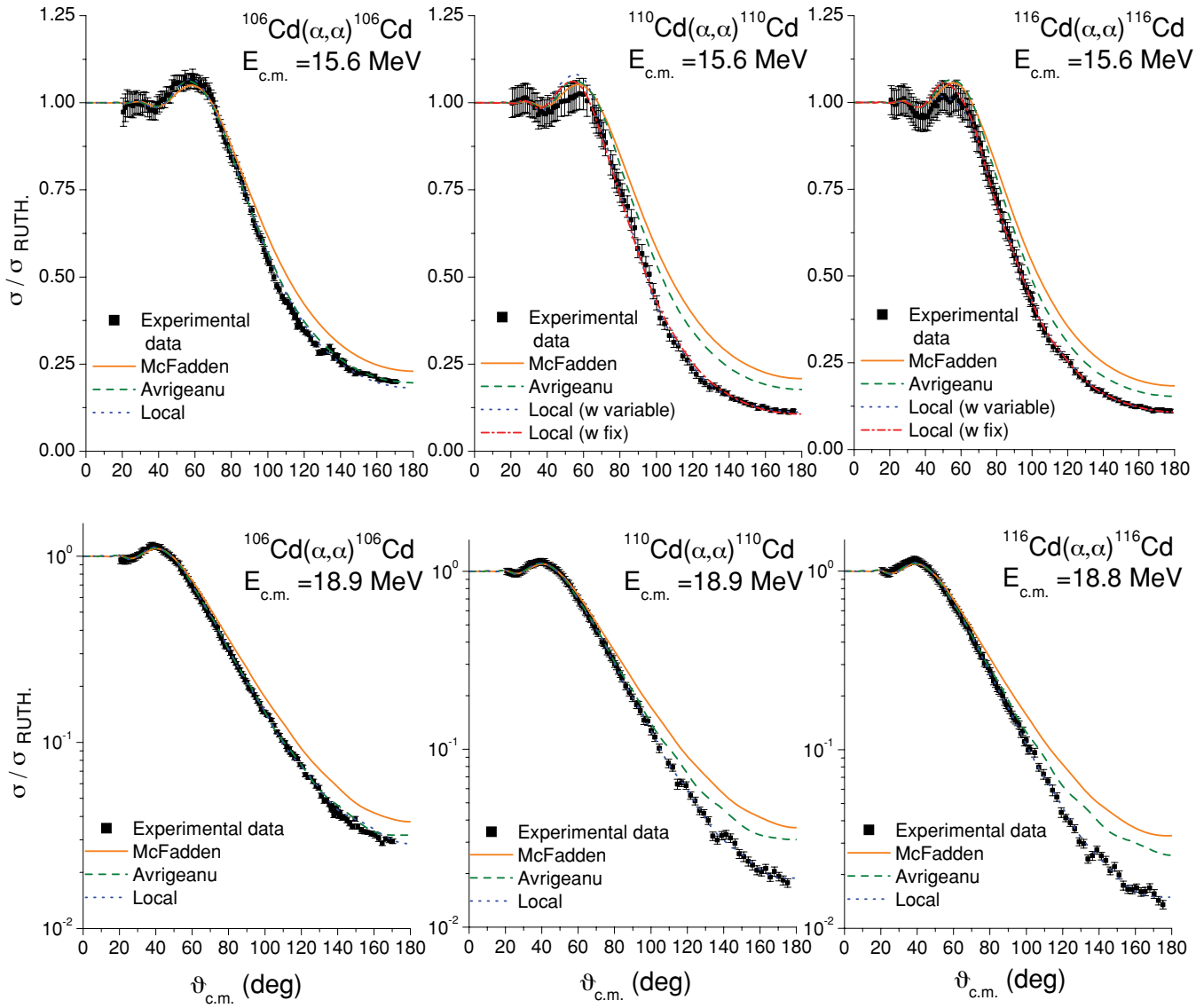

FIG. 4. (Color online) Rutherford-normalized elastic scattering cross sections of the ^{106,110,116}Cd(α,α)^{106,110,116}Cd reaction at E_{cm} = 15.6 MeV (^{106,110,116}Cd), 18.9 MeV (^{106}Cd) and 18.8 MeV (^{110,116}Cd) versus the angle in center-of-mass frame. The lines correspond to the predictions using the present local, regional [43], and global [45] optical potential parameter sets. The ^{106}Cd(α,α)^{106}Cd data were taken from [20,21]. For more information see Secs. III and IV.

and ^{116}Cd can be well described using only a surface imaginary potential. The obtained angular distributions are compared to the experimental results (see Sec. IV) and predictions from global potentials in Fig. 4, and the parameters of the fits are listed in Table II.

It is well known that there are ambiguities in the determination of the optical potential at energies around and especially below the Coulomb barrier. We do not consider here the so-called family problem, which means that almost identical angular distributions are calculated from potentials where the depth of the real part is increased or decreased in discrete steps by about 30%. This problem has been discussed in detail in [18], and its influence on α-induced reaction cross sections for ^{106}Cd will be one focus of the separate study of ^{106}Cd [28]. We restrict ourselves here to real potentials with $J_R \approx 350$ MeV fm^3; these volume integrals are consistent with results that are derived at higher energies without ambiguities [38].

With the above restriction for the volume integral J_R, the angular distributions at 19 MeV can be fitted satisfactorily. The reproduction of the data is excellent and, as expected, χ^2/F values below 1.0 are found. The width parameters remain very close to unity (deviation less than 1%). The strength parameters λ and the resulting volume integrals J_R are slightly larger by a few percent than those found for neighboring semimagic nuclei. The imaginary parts have volume integrals around $J_I \approx 80 - 90$ MeV fm^3, again somewhat larger than for neighboring semimagic nuclei. Such a behavior is expected from the larger absorption and increased reaction cross section; e.g., the total reaction cross sections σ_{reac} around 19 MeV are about 10%

TABLE II. Parameters of the local optical potential. The α optical potential parameters of the ^{106}Cd and ^{112}Sn nuclei are taken from [20,22].

		Real part				Imaginary part									
Nucleus	E_{cm} (MeV)	λ	w	J_R (MeV fm^3)	$r_{R,rms}$ (fm)	W_V (MeV)	r_V (fm)	a_V (fm)	W_S (MeV)	r_s (fm)	a_s (fm)	J_I (MeV fm^3)	$r_{I,rms}$ (fm)	σ_{reac} (mb)	χ^2/F
^{110}Cd	15.6	1.195	1.046	362.3	5.495		–		32.1	1.563	0.344	71.4	7.617	456	0.51
		1.557	1.000[a]	411.9	5.251		–		29.8	1.223	0.682	83.3	6.473	506	0.70
	18.8	1.389	0.995	362.2	5.226		–		32.5	1.380	0.484	80.0	6.893	788	0.32
^{116}Cd	15.6	1.602	0.955	367.8	5.067		–		19.2	0.613	1.291	37.9	5.914	609	0.22
		1.441	1.000	379.2	5.303		–		20.8	1.303	0.677	63.8	6.916	536	0.27
	18.8	1.348	1.001	356.1	5.310		–		39.4	1.366	0.472	90.8	6.928	832	0.61
^{106}Cd	15.6	1.378	0.987	367.9	5.164	–2.9	1.748	0.347	84.8	1.263	0.207	90.9	6.127	349	1.21
	18.9	1.370	0.987	365.7	5.164	–2.9	1.748	0.347	84.8	1.263	0.207	90.9	6.127	749	1.43
^{112}Sn	18.8	1.226	1.004	340.6	5.261	–3.1	1.737	0.341	89.1	1.252	0.218	97.2	6.192	695	0.77

[a]Fixed.

smaller for the semimagic even-even nuclei ^{112,124}Sn (see [40]) compared to nonmagic even-even ^{106,110,116}Cd.

Unfortunately, the situation changes for the angular distributions at 16 MeV. Here the best-fit potentials require width parameters w that deviate by about 5% from unity ($w = 1.046$ for ^{110}Cd, $w = 0.955$ for ^{116}Cd). However, the fit quality remains almost the same if the width parameter w is kept fixed at $w = 1.0$. So it must be noted that the angular distributions at 16 MeV are not sufficiently sensitive to the width parameter w of the potential. Instead, the fits provide a so-called one-point potential [18,26,41,42]. The smaller (larger) width parameter w is compensated by a larger (smaller) strength parameter λ leading to a fixed potential depth at a large radius (e.g., a value $R_{0.2}$ where the real potential depth is 0.2 MeV is derived in [26] from the analysis of elastic scattering excitation functions). We show two calculations in Fig. 4 using the adjusted values for w and using the fixed value $w = 1.0$; the parameters of both calculations are also listed in Table II. Although the differences between the two calculations are small, it must be noted that the derived total reaction cross sections σ_{reac} differ by about 10%. Because the width parameter w is nicely determined to be close to unity from the 19-MeV data, we prefer the total reaction cross sections from the calculations with $w = 1.0$ ($\sigma_{reac} =$ 506 mb for ^{110}Cd and 536 mb for ^{116}Cd) and we assign an uncertainty of 10% for σ_{reac} from the 16 -MeV data. The total cross sections at 19 MeV are well defined with an uncertainty of about 3% (for discussion of uncertainties, see also [40]).

In addition to the above two calculations with the adjusted width parameter w and the fixed $w = 1.0$, a third calculation has been performed using the potential that was derived at the higher energy of 19 MeV. For both ^{110}Cd and ^{116}Cd it is found that the calculated cross sections at backward angles are slightly larger than the experimental values. This clearly indicates that a slight energy dependence of the potential is required to reproduce the angular distributions at both energies.

Further restrictions on the α-nucleus potential can be derived from the analysis of excitation functions (see Sec. V).

IV. GLOBAL OPTICAL MODEL PREDICTIONS

In the present work the following open access regional and global α-nucleus optical potential parametrizations are considered: the recent regional potential of Avrigeanu *et al.* [43] and the global potential of McFadden and Satchler [45].

The regional optical potential (ROP) of Avrigeanu *et al.* [48] was derived starting from a semimicroscopic analysis, using the double-folding model [49], based on α-particle elastic scattering on A $\approx$ 100 nuclei at energies below 32 MeV. The energy-dependent phenomenological imaginary part of this semimicroscopic optical potential also takes into account a dispersive correction to the microscopic real potential. A small revision of this ROP and especially the use of local parameter sets was able to describe the variation of the elastic scattering cross sections along the Sn isotopic chain [50]. A further step to include all available α-induced reaction cross sections below the Coulomb barrier has recently been carried out [43]. First, the ROP based entirely on α-particle elastic scattering [48] was extended to $A \sim$ 50–120 nuclei and energies from $\sim$13 to 50 MeV. Secondly, an assessment of available (α,γ), (α,n), and (α,p) reaction cross sections on target nuclei ranging from ^{45}Sc to ^{118}Sn at incident energies below 12 MeV was carried out. In the present study we use the potential from a review paper (see Table III) [43]. A minor revision of this potential has been suggested very recently in [44].

The global potential of McFadden and Satchler [45] is fitted to the numerous α elastic scattering experiments done on nuclei between O and U at α energies of 24.7 MeV in the 1960s. Fits were obtained using a four-parameter Woods-Saxon potential. This simple potential is widely used for reaction rate calculations and for p process reaction flow simulations [47].

The results of the model calculations are compared with the experimental data in Figure 4. For a strict comparison between the potentials a χ^2 analysis has been done. The resulting χ^2 parameters can be found in Table IV.

It is interesting to note that the ROP of [43] is almost perfect for the ^{106}Cd case whereas it slightly overestimates the elastic scattering cross sections at backward angles for ^{110,116}Cd. This is also seen in the analysis of the backward angle excitation functions (see Sec. V). It is obvious that evolution of the cross sections along the cadmium isotopic chain cannot be reproduced exactly by the ROP under these circumstances. Nevertheless, as discussed in detail in Sec. VI, the cross section

TABLE III. Regional optical potential parameters calculated from Table 3 of [43].

		Real part			Imaginary part						
Nucleus	E_{cm} (MeV)	V_R (MeV)	r_R (fm)	a_R (fm)	W_V (MeV)	r_V (fm)	a_V (fm)	W_S (MeV)	r_s (fm)	a_s (fm)	σ_{reac} (mb)
^{110}Cd	15.6	–134.2	1.367	0.636	–6.2	1.34	0.50	21.6	1.52	0.374	377
	18.8	–125.7	1.405	0.602	–9.8	1.34	0.50	16.9	1.52	0.374	773
^{116}Cd	15.6	–134.0	1.367	0.637	–6.0	1.34	0.50	21.9	1.52	0.368	418
	18.8	–125.6	1.406	0.602	–9.6	1.34	0.50	17.3	1.52	0.368	821
^{106}Cd	15.6	–134.4	1.367	0.635	–6.4	1.34	0.50	21.4	1.52	0.379	348
	18.9	–125.5	1.407	0.600	–10.1	1.34	0.50	16.5	1.52	0.379	754
^{112}Sn	18.8	–125.9	1.406	0.601	–9.8	1.34	0.50	17.0	1.52	0.372	706

ratios are very sensitive to the chosen potential, and thus these ratios are able to provide some hints on possible improvements of the ROP.

V. EXCITATION FUNCTIONS AT BACKWARD ANGLES

Excitation functions of elastic scattering at very backward angles have been measured by three groups [25–27]. Numerical data are not available, and all data have to be read from the given figures in [25–27]. Ref. [25] studies only ^{110}Cd, and the figure is hard to decipher. So we restrict ourselves here to the excitation functions in Refs. [26,27]: Badawy *et al.* [26] have measured excitation functions at the very backward angle of $\vartheta_{lab} = 178.6^\circ \approx \vartheta_{cm}$ from about 10.5 MeV to 15.5 MeV in the cm system. Miller *et al.* [27] show data at $\vartheta_{lab} = 175^\circ$ from about 9.5 MeV to 16.5 MeV. Because the Rutherford-normalized cross section at very backward angles is almost constant, we present both data sets at 175° [27] and 178.6° [26] in a common figure (the calculated deviations because of the different angles remain below 1% in the whole energy range shown in Fig. 5). In addition, we add the most backward data point from our angular distributions, which is also at approximately 175°.

As already pointed out in [26], it is impossible to derive an optical potential from an excitation function at one particular angle. Instead, it is only possible to determine an approximate strength of the imaginary potential and a so-called one-point potential for the real part. Nevertheless, the excitation functions provide additional information and global potentials should be able to reproduce the measured excitation functions. In the following we compare the predictions from the local potentials (without further adjustment to the experimental data of the excitation function) and from the global potentials [43,45] to the experimental data [26,27].

For ^{110}Cd the agreement between the experimental data of [26] and [27] is not good; the data of [26] are slightly higher than the data of [27]. The result from the present analysis of the full angular distribution is a few percent lower than [27]. It must be noted that the above discrepancies may, at least partly, be assigned to the uncertainty of the extraction of the data from figures in [26,27].

The 19-MeV local potential reproduces the excitation function in general quite well, but slightly overestimates our lower data point at 15.6 MeV. The 16-MeV local potential with the unusual width parameter $w = 1.046$ can be excluded because of its strange energy dependence and the strong overestimation of our 18.8-MeV data point. The 16-MeV local potential with the standard width $w = 1$ slightly underestimates the whole excitation function but shows a regular energy dependence (similar to the 19-MeV local potential).

Both global and regional potentials also provide a regular energy dependence; as already seen in the analysis of the angular distributions in Fig. 4, both potentials overestimate the experimental data at backward angles and thus also the excitation functions. The potential of [43] is closer to the data than the old standard potential from McFadden and Satchler [45].

For ^{116}Cd the data of [26] and [27] are in better agreement. Again, our data point at 15.6 MeV is slightly lower than the excitation function by [27]. The theoretical results are very similar to the ^{110}Cd case. Again, the 19-MeV local potential nicely reproduces the data. The 16-MeV local potential with the unusual width $w = 0.955$ shows an oscillatory energy dependence, which is not visible in the experimental data, and it underestimates the excitation function at very low energies. The 16-MeV local potential with $w = 1$ reproduces the smooth energy dependence and gives slightly smaller cross sections than the 19-MeV potential.

TABLE IV. χ^2_{red} of predictions using different global and regional parametrizations compared with the angular distributions studied in this paper.

Parametrization	^{110}Cd(α,α)		^{116}Cd(α,α)		^{106}Cd(α,α)		^{112}Sn(α,α)	Ref.
	15.6 MeV	18.9 MeV	15.6 MeV	18.8 MeV	15.6 MeV	18.8 MeV	18.8 MeV	
Local	0.51–0.70	0.32	0.22–0.27	0.61	1.21	1.43	0.77	this paper
Avrigeanu	40.8	23.8	16.1	42.1	2.44	2.14	2.25	[43]
McFaddden	85.8	62.9	45.8	103.0	38.8	54.2	61.3	[45]

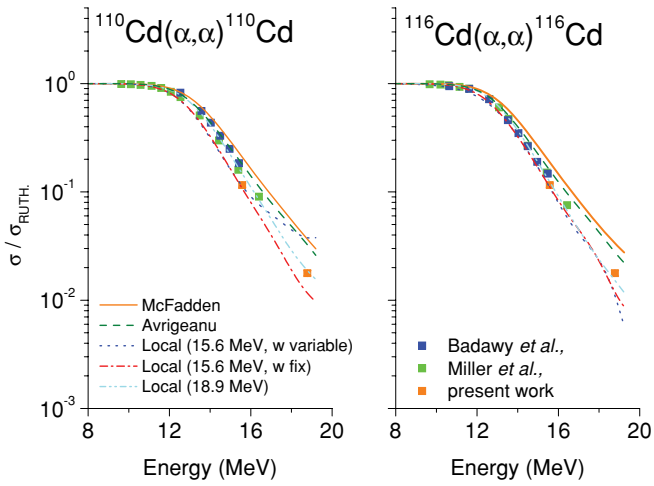

FIG. 5. (Color online) Excitation function of ^{110}Cd$(\alpha,\alpha)^{110}$Cd (left) and ^{116}Cd$(\alpha,\alpha)^{116}$Cd (right) reactions. Experimental data are taken from [26,27]. See text for further discussion.

Both global and regional potentials reproduce again the smooth energy dependence of the data but overestimate the absolute scale. The potential of [43] is again closer to the data than [45].

VI. VARIATION OF THE SCATTERING CROSS SECTION ALONG ISOTOPIC AND ISOTONIC CHAINS

Recently, the variation of the elastic scattering cross sections along the Sn isotopic chain has been studied by Galaviz *et al.* [22]. Complete angular distributions of the ^{112,124}Sn$(\alpha,\alpha)^{112,124}$Sn reactions at $E_{\rm lab} = 19.51$ MeV were measured. It was found that the ratio of the elastic α scattering cross sections of the ^{112}Sn and ^{124}Sn at backward angles shows an oscillation feature. It was evident that the global α-nucleus potentials failed to reproduce either the amplitude and/or the phase of the oscillation pattern for backward angles [22]. This behavior is very similar to the ratio of the Rutherford-normalized cross sections of the ^{92}Mo$(\alpha,\alpha)^{92}$Mo and ^{89}Y$(\alpha,\alpha)^{89}$Y derived by Kiss *et al.* [24].

In the present work, first, the behavior of the elastic α scattering cross sections along the Cd isotopic ($Z = 48$) chain is investigated at $E_{\rm cm} \approx 15.6$ and 18.8 MeV. Although there are small differences in the center-of-mass energies ($\leqslant 120$ keV), the ratios of the Rutherford-normalized cross sections are well defined because the dominating $1/E^2$ dependence of the scattering cross section is taken into account during Rutherford normalization. Therefore, the ratios of Rutherford-normalized cross sections are a very sensitive test for local, regional, and global α-nucleus potential parametrizations. It is found that the ratio of the normalized scattering cross sections shows an oscillation pattern at backward angles (see Fig. 6) similarly to the variation of the elastic scattering cross sections along the Sn isotopic chain [22]. The large number of experimental points and the low uncertainties on all data sets provide a unique probe to understand the evolution of the α-nucleus potential along the Cd isotopic chain.

Moreover, the variation of the elastic α scattering cross sections along the $N = 62$ isotonic chain is also studied by investigating the ratio of the ^{110}Cd$(\alpha,\alpha)^{110}$Cd and ^{112}Sn$(\alpha,\alpha)^{112}$Sn reaction cross sections at $E_{\rm cm} \approx 18.8$ MeV (see Fig. 7). The ^{112}Sn$(\alpha,\alpha)^{112}$Sn is taken from [22]. It was found that the ratio of the elastic scattering cross sections along the $N = 62$ isotonic chain shows a similar behavior to the one reported in [24].

In Figs. 6 and 7 the experimental ratio of the Rutherford-normalized elastic scattering cross sections is compared to the corresponding results of the regional potential of Avrigeanu *et al.* [43] and the global potential of McFadden and Satchler [45]. The gray shaded error band is a very conservative estimate, which is derived from the total errors (statistical and systematic, see discussion in Sec. II) of the measured cross sections in Fig. 4. If we consider only the statistical uncertainties, it can be clearly seen that the oscillatory patterns in the cross section ratios are well defined by the experimental data. (Note that the systematic uncertainty cancels out in the ratio to a large extent.) Figures 6 and 7 show that no regional or global parametrization can describe correctly the amplitude and the phase of the oscillation pattern of the experimental data at backward angles. This fact clearly indicates that the available theoretical α-nucleus optical potential parametrizations have to be further improved.

A closer look at the ratios shown in Figs. 6 and 7 and the underlying cross sections in Fig. 4 provides deeper insight into the reasons for the failure of the potentials and should lead to suggestions for improvements, in particular for the regional potential by Avrigeanu *et al.* [43] with its careful parametrization of all the parameters of the potential in dependence on the target mass number A, charge number Z, and energy E. It is obvious that the mass- and energy-independent global potential by McFadden and Satchler [45] does a good job, but improvements within this very limited parameter space are almost impossible. Therefore, the following discussion focuses mainly on the ROP potential.

The ROP potential is able to reproduce the angular distributions for ^{106}Cd almost perfectly, and thus it also reproduces the total reaction cross section $\sigma_{\rm reac}$ for ^{106}Cd. The elastic scattering cross sections of ^{110}Cd and ^{116}Cd are significantly smaller at backward angles; this corresponds to a significantly larger $\sigma_{\rm reac}$. The increase of $\sigma_{\rm reac}$ with the neutron number can be understood easily because of the dominance of the (α,n) reaction channel and its increasing cross section with increasing neutron number. However, it is surprising that there is a strong change from ^{106}Cd to ^{110}Cd and only a much smaller change from ^{110}Cd to ^{116}Cd: The ratio of elastic scattering cross sections at backward angles is about 1.5 for ^{106}Cd/^{110}Cd whereas it is only about 1.25 for ^{110}Cd/^{116}Cd. Any global potential with a smooth mass dependence such as, for example, Ref. [43], or a missing mass dependence [45] will fail to reproduce the cross section ratios in Fig. 6; the calculated ratios are about 1.1 in all cases and smaller than the experimental results. The apparently different behavior of ^{106}Cd may be understood from a weak subshell closure of the $g_{7/2^+}$ neutron shell at $N = 58$. Although one textbook reference of the shell model [46] shows in its Fig. 1 that the

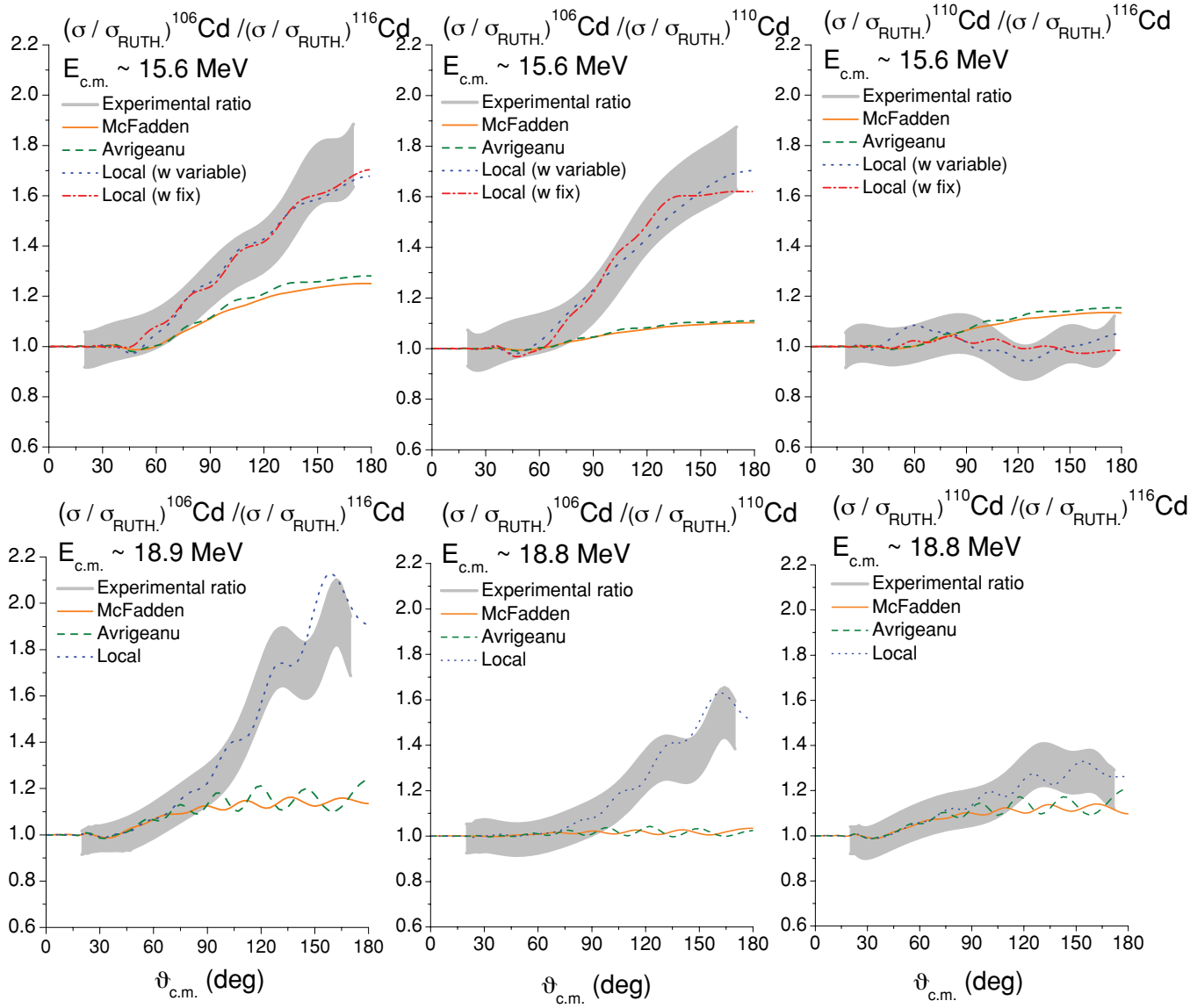

FIG. 6. (Color online) Experimental ratio (gray area with the experimental uncertainties taken into account) of the measured scattering cross sections at ≈ 15.6 MeV (^{106}Cd/^{116}Cd, ^{106}Cd/^{110}Cd, ^{110}Cd/^{116}Cd), 18.9 MeV (^{106}Cd/^{116}Cd), and 18.8 MeV [^{106}Cd/^{110}Cd and (^{110}Cd/^{116}Cd)] versus the angle in center-of-mass frame. The cross sections of the ^{106}Cd(α,α)^{106}Cd are taken from [20,21]. The lines correspond to the predictions using the present local, regional [43], and global [45] optical potential parameter sets. For more information see Secs. III and IV.

$d_{5/2^+}$ subshell is slightly lower than the $g_{7/2^+}$ subshell (and thus one should find a subshell closure at $N = 56$ instead of $N = 58$), there is some evidence from the ground state spins of $J = 5/2^+$ for neighboring $N = 59$ nuclei like ^{105}Pd, ^{107}Cd, and ^{109}Sn that the $g_{7/2^+}$ neutron subshell is filled at $N = 58$. Note that the lowering of the $g_{7/2^+}$ subshell below the $d_{5/2^+}$ subshell is well established for the proton subshells [46]. This weak subshell closure may explain the relatively small total reaction cross section of ^{106}Cd.

The experimental ratio of elastic scattering cross sections at backward angles is about 0.5 between ^{110}Cd and ^{112}Sn. Again, this can be understood, but the argument is different: The neutron numbers are the same for ^{110}Cd and ^{112}Sn and cannot have strong impact on the (α,n) or total reaction cross section. However, ^{112}Sn is a semimagic nucleus with $Z = 50$, and thus the total reaction cross section σ_{reac} is smaller compared to neighboring nuclei, and the elastic scattering cross section is larger. Again, such a behavior cannot be reproduced by any potential with a smooth (or even missing) mass dependence.

This leads to the following recommendations for improvements. In addition to a smooth dependence on the mass number A and charge number Z, a further dependence on shell closures (e.g., parametrized by the distance to a closed shell) should be included in global parametrizations of α-nucleus potentials. This may be complemented by a further dependence of the neutron-to-proton ratio N/Z. The above recommendation may be also interpreted as a guide to the experimentalist for further experiments on nonmagic nuclei. Note that only very few data on nonmagic nuclei have entered into the determination of the

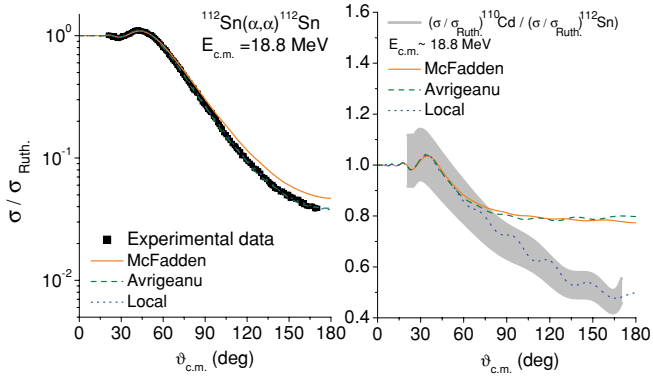

FIG. 7. (Color online) Rutherford-normalized elastic scattering cross sections of ^{112}Sn(α,α)^{112}Sn reaction at $E_{cm} = 18.8$ MeV (left side). Experimental ratio of the scattering cross sections $(\sigma/\sigma_{RUTH})^{110}$Cd / $(\sigma/\sigma_{RUTH})^{112}$Sn at $E_{cm} \approx 18.8$ MeV (gray area with the experimental uncertainty taken into account) versus the angle in center-of-mass frame. The cross sections of the ^{112}Sn(α,α)^{112}Sn are taken from [22]. The lines correspond to the predictions using the present local, regional [43], and global [45] optical potential parameter sets. For more information see Secs. III and IV.

global potential [43] above $A > 80$ (see their Table II). This may also explain that [43] nicely reproduce the data for the semimagic ^{112}Sn but is not able to describe the data for the nonmagic ^{110,116}Cd with the same accuracy.

VII. SUMMARY

In the present work angular distributions of elastically scattered α particles on ^{110,116}Cd have been measured at $E_{lab} = 16.14$ MeV and 19.46 MeV to provide a sensitive test for global parametrizations of the α-nucleus potential used in p process network calculations. The measured data cover the full angular range and have small uncertainties of about 3–4 % over the whole angular range.

A local fit to the angular distributions using a folding potential in the real part and a surface Woods-Saxon imaginary part reproduces all measured angular distributions with high accuracy ($\chi^2/F < 1$). The volume integrals are slightly higher than for neighboring semimagic nuclei. The best-fit potential at 16 MeV shows an unusual width parameter for ^{110}Cd and ^{116}Cd and does not describe the measured excitation functions at backward angles. Very similar fits (also with $\chi^2/F < 1$) can be obtained using the standard width $w = 1$.

The regional and global potentials by [43] and [45] are able to describe the angular distributions with relatively small deviations although both global potentials overestimate the data at backward angles. In all cases the new potential by [43] is closer to the experimental data than the potential of [45]. The same conclusion is found for the excitation functions at backward angles that are available from literature [26,27]. However, the situation becomes worse for the evolution of the potentials along isotopic and isotonic chains. The measured ratio of cross sections cannot be reproduced by any regional and global potential because the deviations at backward angles are amplified in the ratios. A reason for this problem may be the influence of shell closures, which are not taken into account in the parametrizations of [43] or [45].

Since modeling explosive nucleosynthesis scenarios requires reaction rates on a large number of reactions involving thousands of nuclei, the α-nucleus potential has to be known in a wide region. The reliability of the extrapolation to unstable nuclei has to be tested by measuring the elastic scattering cross sections on several nuclei along isotopic and isotonic chains. The ratio of Rutherford-normalized cross sections along isotopic or isotonic chains is a very sensitive observable for the quality of α-nucleus potentials, and it should be used in further work to restrict global parametrizations of α-nucleus potentials.

Further systematic experimental elastic α scattering studies at energies around the Coulomb barrier are essential, in particular on intermediate mass and heavy nuclei without shell closures. The experimental scattering data should be complemented by data on α-induced reaction cross sections in the same energy region. Scattering and reaction data have to enter into theoretical studies leading eventually to a robust global α-nucleus potential that is able to describe all observables with reasonable accuracy.

ACKNOWLEDGMENTS

This work was supported by the EUROGENESIS research program, by the Hungarian Office of the National Scientific Research Fund (OTKA), Grants No. NN83261 and No. K068801, by the European Research Council, Grant No. 203175, and by the Joint Institute for Nuclear Astrophysics (NSF Grant No. PHY0822648). G.G.K. and D.G. acknowledge the support of the Spanish Interministerial Commission of Science and Technology, under Project No. FPA2005-02379, and the Ministry of Education and Science (MEC) Consolider, Project No. CSD2007-00042. G.G. acknowledges support from the Bolyai grant. D.G. acknowledges support from the Spanish Ministry of Science Juan de la Cierva grant. This work was also supported by the Scientific and Technological Research Council of Turkey (TUBITAK), Grants No. 108T508 (TBAG1001) and No. 109T585 (under the EUROGENESIS research program). Fruitful discussions with M. Avrigeanu are gratefully acknowledged.

[1] S. E. Woosley and W. M. Howard, Astrophys. J. Suppl. **36**, 285 (1978).
[2] M. Arnould and S. Goriely, Phys. Rep. **384**, 1 (2003).
[3] T. Rauscher, Phys. Rev. C **73**, 015804 (2006).
[4] W. Rapp, J. Görres, M. Wiescher, H. Schatz, and F. Käppeler, Astrophys. J. **653**, 474 (2006).

[5] T. Rauscher, arXiv:1010.4283.
[6] C. Nair, A. R. Junghans, M. Erhard, D. Bemmerer, R. Beyer, E. Grosse, K. Kosev, M. Marta, G. Rusev, K. D. Schilling, R. Schwengner, and A. Wagner, Phys. Rev. C **81**, 055806 (2010).
[7] P. Mohr, Zs. Fülöp, and H. Utsunomiya, Eur. Phys. J. A **32**, 357 (2007).
[8] T. Rauscher, G. G. Kiss, Gy. Gyürky, A. Simon, Zs. Fülöp, E. Somorjai, Phys. Rev. C **80**, 035801 (2009).
[9] Zs. Fülöp, Á. Z. Kiss, E. Somorjai, C. E. Rolfs, H. P. Trautvetter, T. Rauscher, and H. Oberhummer, Z. Phys. A **355**, 203 (1996).
[10] W. Rapp, M. Heil, D. Hentschel, F. Käppeler, R. Reifarth, H. J. Brede, H. Klein, and T. Rauscher, Phys. Rev. C **66**, 015803 (2002).
[11] Gy. Gyürky, G. G. Kiss, Z. Elekes, Zs. Fülöp, E. Somorjai, A. Palumbo, J. Görres, H. Y. Lee, W. Rapp, M. Wiescher, N. Özkan, R. T. Güray, G. Efe, and T. Rauscher, Phys. Rev. C **74**, 025805 (2006).
[12] N. Özkan, G. Efe, R. T. Güray, A. Palumbo, J. Görres, H. Y. Lee, L. O. Lamm, W. Rapp, E. Stech, M. Wiescher, Gy. Gyürky, Zs. Fülöp, and E. Somorjai, Phys. Rev. C **75**, 025801 (2007).
[13] I. Cata-Danil, D. Filipescu, M. Ivascu, D. Bucurescu, N. V. Zamfir, T. Glodariu, L. Stroe, G. Cata-Danil, D. G. Ghita, C. Mihai, G. Suliman, and T. Sava, Phys. Rev. C **78**, 035803 (2008).
[14] C. Yalcin, R. T. Güray, N. Özkan, S. Kutlu, Gy. Gyürky, J. Farkas, G. G. Kiss, Zs. Fülöp, A. Simon, E. Somorjai, and T. Rauscher, Phys. Rev. C **79**, 065801 (2009).
[15] E. Somorjai, Zs. Fülöp, Á. Z. Kiss, C. E. Rolfs, H. P. Trautvetter, U. Greife, M. Junker, S. Goriely, M. Arnould, M. Rayet, T. Rauscher, and H. Oberhummer, Astron. Astrophys. **333**, 1112 (1998).
[16] Gy. Gyürky, Z. Elekes, J. Farkas, Zs. Fülöp, Z. Halász, G. G. Kiss, E. Somorjai, T. Szücs, R. T. Güray, N. Özkan, C. Yalcin and T. Rauscher, J. Phys. G. **37**, 115201 (2010).
[17] G. G. Kiss, T. Rauscher, T. Szücs, Zs. Kertész, Zs. Fülöp, Gy. Gyürky, C. Fröhlich, J. Farkas, Z. Elekes, and E. Somorjai, Phys. Lett. B. **695**, 419 (2011).
[18] P. Mohr, T. Rauscher, H. Oberhummer, Z. Máté, Zs. Fülöp, E. Somorjai, M. Jaeger, and G. Staudt, Phys. Rev. C **55**, 1523 (1997).
[19] Zs. Fülöp, Gy. Gyürky, Z. Máté, E. Somorjai, L. Zolnai, D. Galaviz, M. Babilon, P. Mohr, A. Zilges, T. Rauscher, H. Oberhummer, and G. Staudt, Phys. Rev. C **64**, 065805 (2001).
[20] D. Galaviz, Ph.D. thesis, TU Darmstadt, 2004.
[21] G. G. Kiss, Zs. Fülöp, Gy. Gyürky, Z. Máté, E. Somorjai, D. Galaviz, A. Kretschmer, K. Sonnabend, and A. Zilges, Eur. Phys. J. **27**, 197 (2006).
[22] D. Galaviz, Zs. Fülöp, Gy. Gyürky, Z. Máté, P. Mohr, T. Rauscher, E. Somorjai, and A. Zilges, Phys. Rev. C **71**, 065802 (2005).
[23] A. Palumbo, W. Tan, J. Görres, M. Wiescher, Zs. Fülöp, Gy. Gyürky, G. G. Kiss, E. Somorjai, D. Galaviz, N. Özkan, R. T. Güray, in *Proceedings of Nuclei in the Cosmos-X, Mackinac Island, 2008* [PoS(NIC-X)046 (2008)].
[24] G. G. Kiss, P. Mohr, Zs. Fülöp, D. Galaviz, Gy. Gyürky, Z. Elekes, E. Somorjai, A. Kretschmer, K. Sonnabend, A. Zilges, and M. Avrigeanu, Phys. Rev. C **80**, 045807 (2009).
[25] Y. Eisen, E. Abramson, G. Engler, M. Samuel, U. Smilansky, and Z. Vager, Nucl. Phys. A **236**, 327 (1974).
[26] I. Badawy, B. Berthier, P. Charles, M. Dost, B. Fernandez, J. Gastebois, and S. M. Lee, Phys. Rev. C **17**, 978 (1978).
[27] M. Miller, A. M. Kleinfeld, A. Bockisch, and K. Bharuth-Ram, Z. Phys. A **300**, 97 (1981).
[28] D. Galaviz *et al.* (in preparation).
[29] Z. Máté, S. Szilágyi, L. Zolnai, Å. Bredbacka, M. Brenner, K.-M. Källmann, and P. Manngård, Acta Phys. Hung. **65**, 287 (1989).
[30] G. G. Kiss, D. Galaviz, Gy. Gyürky, Z. Elekes, Zs. Fülöp, E. Somorjai, K. Sonnabend, A. Zilges, P. Mohr, J. Görres, M. Wiescher, N. Özkan, T. Güray, C. Yalcin, and M. Avrigeanu, AIP conf. proc. **1016**, 221 (2008).
[31] D. De. Frenne and A. Negret, Nucl. Data Sheets **109**, 943 (2008).
[32] D. De Frenne and A. Jacobs, Nucl. Data Sheets **89**, 481 (2000).
[33] J. Blachot, Nucl. Data Sheets **92**, 455 (2001).
[34] D. De Frenne and E. Jacobs, Nucl. Data Sheets **79**, 639 (1996).
[35] A. M. Kobos, B. A. Brown, R. Lindsay, and G. R. Satchler, Nucl. Phys. A **425**, 205 (1984).
[36] G. R. Satchler and W. G. Love, Phys. Rep. **55**, 183 (1979).
[37] H. Abele and G. Staudt, Phys. Rev. C **47**, 742 (1993).
[38] U. Atzrott, P. Mohr, H. Abele, C. Hillenmayer, and G. Staudt, Phys. Rev. C **53**, 1336 (1996).
[39] H. de Vries, C. W. de Jager, and C. de Vries, At. Data Nucl. Data Tables **36**, 495 (1987).
[40] P. Mohr, D. Galaviz, Zs. Fülöp, Gy. Gyürky, G. G. Kiss, E. Somorjai, Phys. Rev. C **82**, 047601 (2010).
[41] C. Signorini, A. Andrighetto, M. Ruan, J. Y. Guo, L. Stroe, F. Soramel, K. E. G. Löbner, L. Müller, D. Pierroutsakou, M. Romoli, K. Rudolph, I. J. Thompson, M. Trotta, A. Vitturi, R. Gernhäuser, and A. Kastenmüller, Phys. Rev. C **61**, 061603(R) (2000).
[42] J. P. Fernández-García, M. Rodríguez-Gallardo, M. A. G. Alvarez, and A. M. Moro, Nucl. Phys. A **840**, 19 (2010).
[43] M. Avrigeanu, A. C. Obreja, F. L. Roman, V. Avrigeanu, and W. von Oertzen, At. Data Nucl. Data Tables **95**, 501 (2009).
[44] M. Avrigeanu and V. Avrigeanu, Phys. Rev. C **82**, 014606 (2010).
[45] L. McFadden and G. R. Satchler, Nucl. Phys. **84**, 177 (1966).
[46] P. A. Klinkenberg, Rev. Mod. Phys. **24**, 63 (1952).
[47] T. Rauscher, code NON-SMOKERWEB [http://nucastro.org/websmoker.html].
[48] M. Avrigeanu, W. von Oertzen, A. J. M. Plompen, and V. Avrigeanu, Nucl. Phys. A **723**, 104 (2003); M. Avrigeanu, W. von Oertzen, and V. Avrigeanu, *ibid.* **764**, 246 (2006).
[49] D. T. Khoa, W. von Oertzen, and H. G. Bohlen, Phys. Rev. C **49**, 1652 (1994).
[50] M. Avrigeanu and V. Avrigeanu, Phys. Rev. C **73**, 038801 (2006).